Low-Profile Frequency-Scanned Antenna Based on Substrate Integrated Waveguide

Xue-Xia Yang, Member, IEEE, Yingjie Yu, Duqi Di, Steven Gao, Senior Member, IEEE

Abstract—A beam scanning flat antenna array with the frequency that covers about the whole X/Ku-band is proposed in this paper. The radiation element is the continuous transverse stub (CTS) constituted by the substrate integrated waveguide (SIW). The CTS array is fed by a linear source which is a SIW parabolic reflector, and good impedance matching characteristics within a broad bandwidth are obtained. The beam steering direction is tunable with the frequency increasing within the operation band. The design principles of the SIW based CTS array and the feed structure are explained in details. One 16-element array is simulated, designed and fabricated. The measurement results show a scanning angle range from 52.2° to -16.8° with the 3-dB gain decreasing within the operation band from 8.5 GHz to 14.1GHz. At the center frequency of 12 GHz, it achieves a maximum gain of 18.1 dBi with an array size of $11.7\lambda_0 \times 1.28\lambda_0$, the first sidelobe level is -11.4 dB and the 3-dB beamwidth is 6.5°.

Index Terms—Frequency-scanned antennas (FSA), continuous transverse stub (CTS), substrate integrated waveguide (SIW), flat array

I. Introduction

Beam scanning antennas are required in many civilian and military applications [1-2]. Frequency-scanned antennas (FSA) have multi-beam steering performance with the frequency varying and do not require any mechanical movement or electrical adjustment. The frequency-scanned reflection grating antenna fed by a linear source achieved 11.9° scanning angle with a bandwidth of 11.1% from 8.5 GHz to 9.5 GHz [3]. The FSA based on the reflector antenna can achieve high gain but it has a bulky size and high cost due to the separated arrangement of the radiator and the feed.

The printed FSA was first investigated in 1979 shortly after the invention of microstrip antennas [4]. However, the antenna gain was low due to the microstrip line loss. A wideband offset slot-coupled patch antenna array covering most X/Ku-band from 8.75 to 12.25 GHz was suggested to apply in multimode radars [5]. The 4×4 array had a beam tilting at 20° by moving the coupling slot within the bandwidth with the maximum gain of 20.6 dBi being achieved. Recently, the printed FSA was developed by using the metamaterials [6-7]. By loading the slow-wave printed meander line, one printed 16-element array achieved a beam scanning range of -27.5°~+46° with the frequency varying from 8.9 to 10.6 GHz and a maximum gain of 15.5 dBi [6]. The tapered composite right/left-handed unit cell sections extended the scanning angle of a leaky-wave antenna to -72°~+75° over a frequency range of 8.0-13.0 GHz [7]. However, the broadside gain of this FSA was only 9.0 dBi with an antenna size of $6.0\lambda_0 \times 0.7\lambda_0$. A simple printed 6-element E-shaped leaky-wave array could scan the beam from -30°~15° with the frequency increasing within 0.93-3.65 GHz range but the gain was only 8.0 dBi [8].

CTS (Continuous Transverse Stub) arrays were invented in early 1990s [9]. The CTSs, periodically arraying on the plane waveguide, are fed by a linear source and act as the radiation elements with leaky-wave radiation. The CTS array operates on the quasi-TEM (i.e. TM_0) mode of the parallel plate waveguide so it has the good features of broadband, high gain, compact size, and light weight. It also could be designed to operate at multi-band and beam steering. The coplanar waveguide (CPW) and the coaxial line were also suggested to be used as the CTS for the same operation mode of TEM [10-12]. The feasibility of CPW-CTS as an antenna was verified by one-element in [10]. The dual-band (4.2 and 19.4 GHz) and triple-band (5.18, 6.536 and 7.51 GHz) operations of the coaxial line CTS arrays were investigated in [11] and [12] with 6-element and 2-element arrays, respectively.

Recently, several CTS beam steering arrays have been proposed. The 3-element leaky-wave CPW-CTS array obtained the scan-angle range from 58° to 124° by changing 6 metamaterial-based phase shifters [13]. Ettorre, et al, designed a Ka-band CTS array with a wide scanning range of ±40° by moving a horn within the focal plane of the pillbox feeding system, which was fabricated by the metal process [14]. By using the substrate integrated waveguide (SIW) technology, Ref. [15] suggested a mechanical beam scanning array with simplified feed structure to lower the profile. A millimeter wave FSA had a scanning range of -43°~3° with the frequency varying within 27-36 GHz range and the highest gain was 16.9 dBi with an aperture size of $13.5\lambda_0 \times 2.1\lambda_0$ [16]. A surface wave antenna with a broadband operation from 6.1 to 18 GHz was designed by a parabolic reflector feed structure [17].

In this paper, a novel frequency-scanned CTS array is proposed by improving the broadband feed structure proposed in [17] into SIW one. The CTS array and the parabolic reflector

Manuscript received December 14, 2015, accepted January 02, 2016.This work is supported by the Natural Science Foundation of China (6127106).

X.-X. Yang, Y.J. Yu, and L.Q. Di are all with the School of Communication and Information Engineering, Shanghai University, Shanghai 200072, China. S. Gao is with the School of Engineering and Digital Arts, University of Kent, UK. X.-X. Yang is also with the Key Laboratory of Specialty Fiber Optics and Optical Access Networks, Shanghai University, Shanghai, China. Corresponding author is X.-X. Yang (email: yang.xx@shu.edu.cn).

are all constituted by the printed SIW. The beam steering function is realized by the different phase of the varying frequency so no phase shifter is required. One 16-element SIW-CTS array is simulated, designed and fabricated. The measured maximum gain is 18.1 dBi and the array size is $11.7\lambda_0 \times 1.28\lambda_0$. The first sidelobe level is -11.4 dBi. This SIW-CTS based flat FSA has advantages such as simple structure, compact size, light weight and low cost, thus it is potentially useful for wireless communications and military applications.

II. SIW-CTS Array Configuration and Design

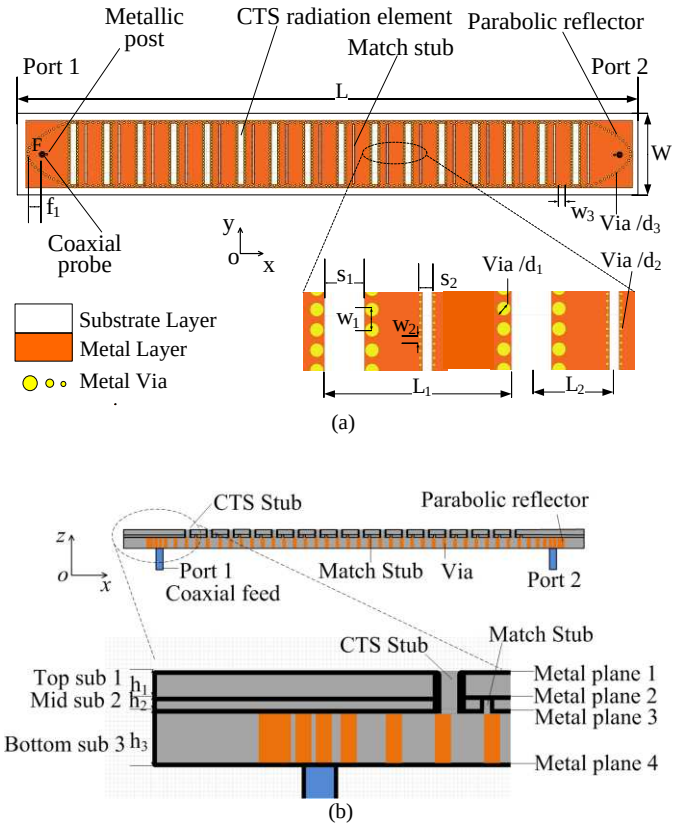

Fig.1 Configuration of the CTS array antenna. (a) top view, (b) side view.

One 16-element SIW-CTS based FSA array is designed and investigated to show the design principle. The configuration of the proposed SIW-CTS based FSA is shown in Fig. 1. It is stacked by three substrate layers. The antenna array consists of 16-element radiation CTSs, 16 impedance matching stubs, and the feed structure of a parabolic reflector fed by a coaxial probe. They are all constituted by the SIW with different sizes of via and space, which are determined by the dielectric substrate and the performance required [18]. The vias for the CTSs cut through the top and the middle substrate layers while those for the match stub are in the middle one. The vias with the same diameter and space as the parabolic reflector surround the whole antenna array, which are in the bottom substrate. As shown in Figure 1, the diameters and spaces of the periodical vias of the CTS radiation stub, the impedance matching stub, and the surrounding are denoted as d_1 and w_1, d_2 and w_2, d_3 and w_3, respectively. The whole size of the array is denoted as L× W.

The lengths of the 16 radiation CTSs and the 16 impedance match stubs are all the width of the antenna array W. The 16-element radiation CTSs are in the top and middle substrate layers with the width of S_1. The height of the CTS is (h_1+h_2), which is the total of the thickness of substrates layers 1 and 2. The impedance match stub beside every CTS is in the middle substrate layer, so the height of the match stub is h_2, which is the thickness of substrate layer 2. The width of the match stub is S_2. The distance L_1 between the radiation stubs of CTS should meet the following condition,

$$L_1 < \frac{\lambda}{1+|\sin\theta_{\max}|} \tag{1}$$

where $\theta_{\max}$ is the maximum scanning angle, and λ is the minimum waveguide wavelength in the free space within the operation band. So the beam steering range has relationship with the operation wavelength, the permeability of the substrate and the array space.

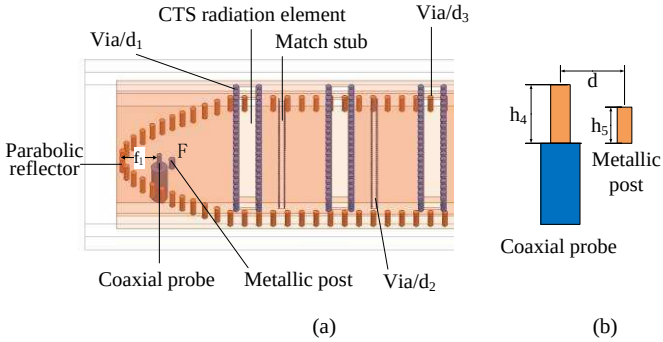

Fig. 2 Configuration of the feed structure.

The feed structure is in the bottom substrate layer and the detailed geometrical structure is plotted in Fig. 2. The feed structure includes a coaxial probe, a metallic post, and a coaxial-to-parallel plate waveguide transition realized by a SIW parabolic reflector. The coaxial probe has a characteristic impedance of 50 Ω and is located at the focus of the parabolic plane with the focal distance of f_1. Fig. 2 (b) illustrates the geometrical sizes of the probe and the metallic post. From the bottom metal plane, the coaxial probe protrudes a height of h_4, which is a little less than the bottom substrate thickness of h_3. The metallic post has a height of h_5, which is less than the coaxial probe height h_4, and is located at a space of d from the probe.

Ports 1 and 2 are set on both sides of the SIW-CTS array as shown in Fig. 1(a). When the signal is excited at port 1, port 2 is terminated to a match load of 50 Ω to absorb the residual wave. The SIW parabolic reflector is formed by a series of vias which constitute a parabolic plane with the height of substrate thickness h_3. When the cylindrical electromagnetic (EM) wave is excited in the bottom substrate layer by the coaxial probe, the forward wave will be suppressed by the metallic post, and the backward waves will be reflected by the parabolic reflecting wall. The metallic post also serves as a matching element to broaden the bandwidth. The EM wave reflected by the SIW reflector propagates as the plate waveguide mode of quasi-TEM in the substrate and will be

radiated by the CTSs progressively as leaky-wave. The remaining EM wave will be absorbed by the match impedance at port 2.

The whole CTS array is surrounded by the same periodically conductive vias as the SIW parabolic reflector to limit the EM wave within the substrates. The performance and parametric analysis of the SIW-CTS based FSA will be investigated in the following section by computer simulations using the commercial tool Ansoft HFSS [19].

III. Performance Analysis and Simulations

The 16-element SIW-CTS antenna array could steer beam with the frequency ranging from 8 to14 GHz. Theoretically, the CTS could radiate the EM wave with any wavelength because of the operation mode of quasi-TEM in the parallel plate waveguide. The CTS array is fed by the linear source which is a SIW parabolic reflector, and this leads to good impedance matching characteristic within a broad frequency range. Thus, a broadband performance of the SIW-CTS antenna array would be derived from the quasi-TEM operation mode in the CTS and the parabolic reflector feed structure. The frequency-scanned performance is realized by the different phase constant β, i.e. $2\pi/\lambda_g$, at the different frequency. λ_g is the waveguide wavelength in the substrate. The performance analysis will be illustrated by the simulation results of HFSS software.

A. CTS Array and Impedance Matching Stub

The CTS operates on quasi-TEM mode of the parallel plate waveguide whose cutoff wave length is infinite. Although any EM wave with various frequency could propagate in the CTS the, there are high order mode, which would interfere the EM field of the main mode of quasi-TEM. To prohibit the first high order mode of TE_1/TM_1, the waveguide wavelength in the substrate at the upper frequency should be higher than two times of the height of the bottom substrate h_3, which is also the CTS width s_1[20]. In this case of 8-14 GHz band and 2.65 permittivity, s_1 is less than 6.6 mm. The size choice of s_1 should also consider the energy radiated by every stub when the stub height, which is the substrate depth of (h_1+h_2), cannot be changed. The planar quasi-TEM wave would be radiated progressively by the CTSs as the leaky wave from the exciting port, port 1.

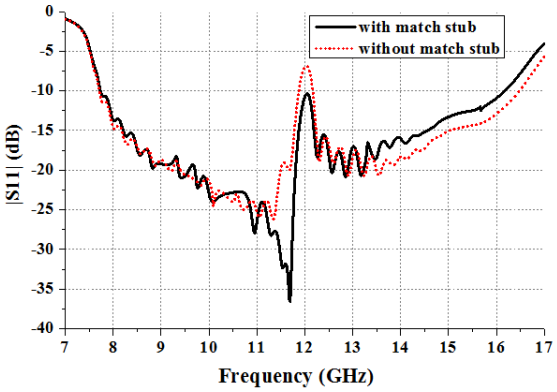

Fig. 3 Simulated reflection coefficient of SIW-CTS array w/o match stub.

Setting a line source of plane wave at the distance of λ_g /4 from the first CTS, the simulated reflection coefficient of the 16-element CTS array is plotted in Fig. 3 by the dot-line. It is shown that $|S_{11}|$ at the center frequency of 12 GHz is high, which could be explained by the operation principle of the CTS array. Fig. 4 illustrates the first two CTSs. There is discontinuous characteristic at every radiation stub. Thus, the reflected wave will occurred except for the radiation and the transmission waves when the input EM wave passes through the first CTS. It is the same with the second and the other CTSs. The distance between the two radiating stubs is one guided wavelength (λ_g) at 12 GHz so the reflected wave to the previous stub is in-phase superposition and the impedance match is deteriorated.

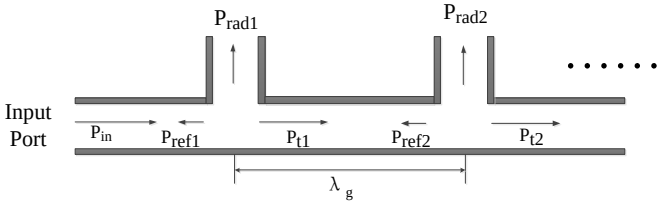

Fig. 4 CTS radiation stub operation principle.

To decrease the reflected EM wave at every CTS and improve the impedance match characteristic, a mini-stub is loaded with a space of L_2 beside every radiation stub. The simulated $|S_{11}|$ with the match stubs is drawn as the solid line in Fig. 3. It can be found that the reflection coefficient at the center frequency decrease apparently and the impedance matching performance is improved. $|S_{11}|$ less than -10 dB covers a broad band from 7.7 to 16.5 GHz with a fractional bandwidth of 73%.

B. Feed Structure Design

To excite the quasi-TEM mode in every continuous transverse stub by a linear source, a parabolic reflector fed by a coaxial line with a metal post is adopted. The parabolic reflector is realized by the metal vias and exhibits broadband performance, which is designed by the operation frequency and the substrate characteristics. The coaxial feedline is located at the focus of the parabolic reflector. The post beside the coaxial feedline not only blocks the electromagnetic wave to the reflector to excite the ideal plane wave, but also improves the impedance characteristic further.

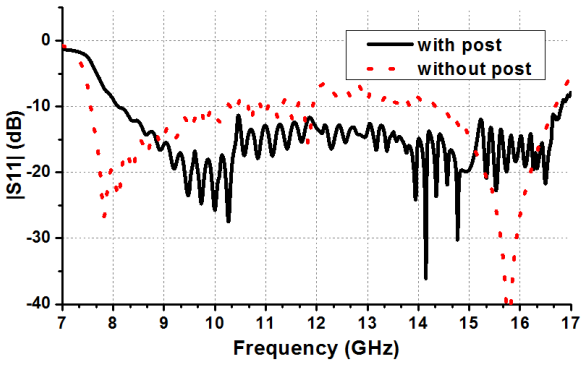

Fig. 5 Simulated reflection coefficient of the SIW-CTS array fed by the parabolic reflector w/o the post.

The reflection coefficient is deeply affected by the location and size of the metallic post. The self-impedance of the metallic post and the mutual impedance between the probe and the post can be adjusted by varying the length, diameter, and location of the post. To illustrate the effectiveness of the metallic post, the reflection coefficient curves of the SIW-CTS array versus the frequency w/o the post are plotted in Fig. 5. It could be seen that $|S_{11}|$ decreases apparently within the broad operation band with the metallic post. The relative bandwidth of |S11| less -10 dB is 69% (8.1-16.8GHz), which is a little narrower than that without the parabolic reflector feed structure.

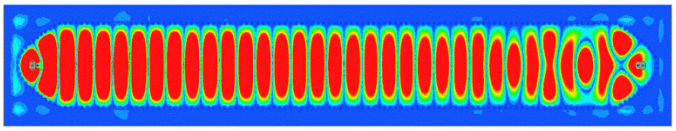

Fig. 6 Electrical field distribution in the bottom substrate layer at 12 GHz.

Fig 6 draws the electrical field strength distribution of the feed structure in the bottom substrate layer. There are two maximum strength values within one waveguide length λ_g. The electrical field strength at every radiating stub is maximum and in-phase. These simulated results show that the parabolic reflecting wall realized by the metal plane in [17] is effective by using SIW structure at X/Ku band.

C. Effectiveness of the Surrounding Vias

The vias surrounding the two sides of radiation CTSs and the impedance matching stubs are designed to limit the EM wave within the CTS length range so that the EM wave is radiated effectively above the CTS. The electrical field strength distribution in the bottom substrate layer without the surrounding vias is drawn in Fig. 7, which shows a little EM wave escape from the two side. The simulation results show that the radiation efficiencies with and without the surrounding vias are 93.2% and 92%, respectively.

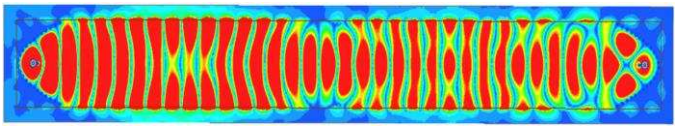

Fig. 7 Electrical field distribution in the bottom substrate layer without the surrounding vias at 12 GHz.

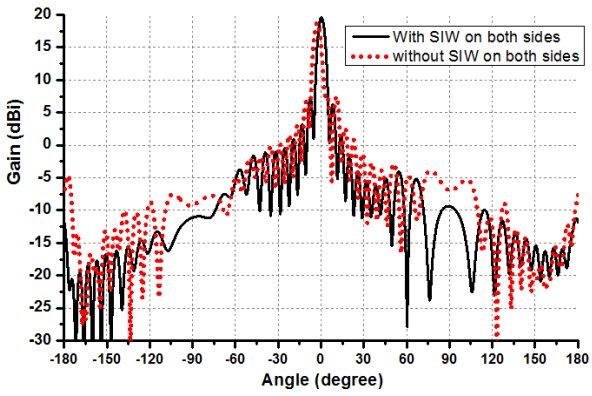

Fig.8 Simulated gain patterns at 12 GHz w/o the surrounding vias.

Fig. 8 compares the gain patterns at 12 GHz with and without the surrounding vias. It can be seen that the gain decreases 0.7dBi and the broadside direction shifts 2.5°. The main reason is that the escaped EM wave from the two ends of every CTS induces the back radiation at 180° and the side radiation at +/- 90°.

D. Beam Scanning Characteristics

The SIW-CTS based FSA structure and the sizes are finally determined. The relative dielectric constant of the substrate is 2.65. The thickness of the three substrates and all of the final geometrical sizes are listed in TABLE I. The distance L_1 between every radiation CTS is 16.15 mm, which is one λ_g at the center frequency of 12 GHz to remain in-phase at every CTS. L_1 is also 0.646 λ_0, which is essential to avoid the sidelobe level in free space.

TABLE I
GEOMETRICAL SIZES OF THE SIW-CTS ARRAY (UNIT: MM)

L	W	h_1	h_2	h_3	L_1	L_2	s_1	s_2	f_1
292.5	32	2.5	0.5	3	16.15	7	3	1	6.5
h_4	h_5	d	w_1	w_2	w_3	d_1	d_2	d_3	/
2.9	1.9	2.3	1.45	0.5	2.5	1.0	0.2	1.0	/

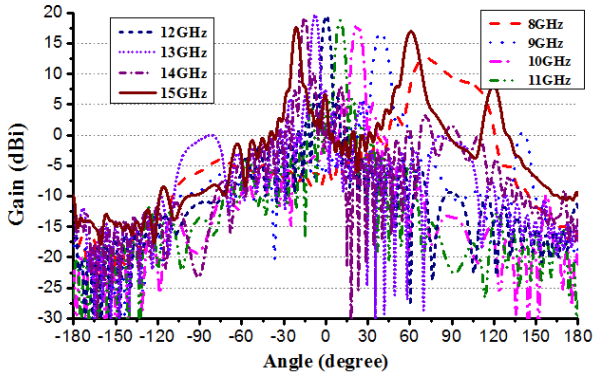

Fig.9 Simulated gain patterns of beam scanning.

The simulated beam steering characteristics versus the frequency are plotted in Fig. 9. The gain at the center frequency of 12 GHz on the broadside of 0° is 19.5 dBi. The maximum directions at 9 and 14 GHz are on the angles of 39.2° and -15.2° with the corresponding gains being 16.8 dBi and 19.2 dBi, respectively. Although the gain at the upper frequency of 15 GHz is 17.6 dBi at the scanning angle of -21.1°, the pattern splits because the condition of formula (1) is not satisfied. At the low frequency of 8 GHz, the gain decreases sharply to 12.6 dBi at the scanning angle of 71.1° and the pattern deteriorates. The 3-dB gain bandwidth is from 9 to 14 GHz with a fractional bandwidth of 43%, which is narrower than that of $|S_{11}|$ less than -10 dB of 69%.

IV. Measurements and Discussion

To verify the results of computer simulations, one 16-element SIW-CTS based FSA array covering X/Ku band is fabricated and measured. Fig. 10 shows the top and bottom of the 1st, the 2nd and the 3rd substrate layers. The complete FSA is obtained by fixing the three substrate layers together using the plastic screws around the four edges of the array antenna. The reflection coefficients are measured by the 8722ES Agilent Vector Network Analyzer and the patterns and gains are measured in the chamber.

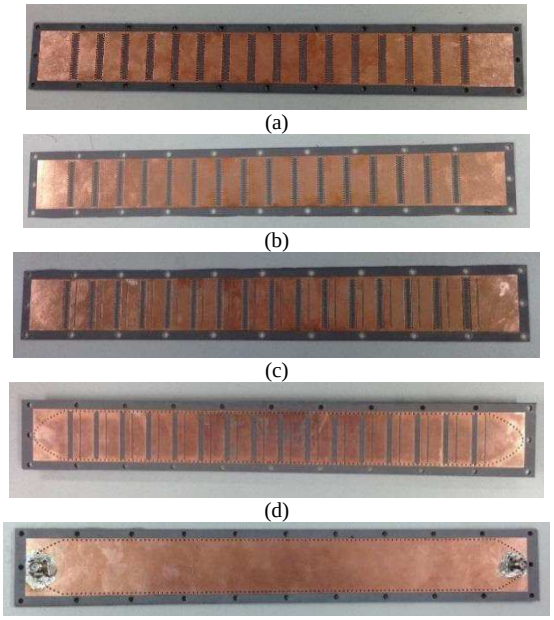

Fig.10 Photos of the fabricated SIW-CTS based FSA array. (a) top and bottom of the 1st substrate, (b) top of the 2nd substrate, (c) bottom of the 2nd substrate, (d) top of the3rd substrate, (e) bottom of the 3rd substrate

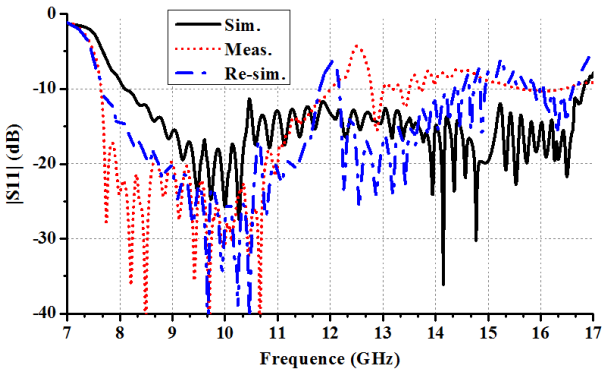

Fig. 11 Simulated and measured reflection coefficient versus frequency.

The dot-line in Fig. 11 plots the measured reflection coefficients versus frequency with the simulated one being drawn in the solid line for comparison. The measured relative bandwidth of $|S_{11}|$ less -10 dB is 44.5% from 7.64 to 12.02 GHz. The $|S_{11}|$ performance deteriorates at the upper bandwidth from 12.02 GHz and the operation band shifts to the low frequency. The error mainly comes from the parameters of the dielectric substrates and the fabrication process. The thicknesses h_1, h_2 and h_3 of the three substrates are measured to be 3.24 mm, 0.57 mm, and 2.59 mm respectively, instead of the given values of 3.0 mm, 0.5 mm and 2.5 mm by the manufacture company. The dash-dot line in Fig. 11 shows the reflection coefficient with the measured substrate thicknesses. It could be seen that the curve trends toward the measured one, which verifies that the plate waveguide height h_3 and the radiation stub height (h_1+h_2) influence the impedance match apparently.

To investigate the influence of the dielectric constant value tolerance of the substrate on the operation frequency, the $|S_{11}|$ versus frequency at different ε_r values of 2.55, 2.65, and 2.75 are compared in Fig. 12. It could be found that operation frequency shift to a lower band with the increasing of ε_r but the influence is not obviously. The manufacture process might also produce the error.

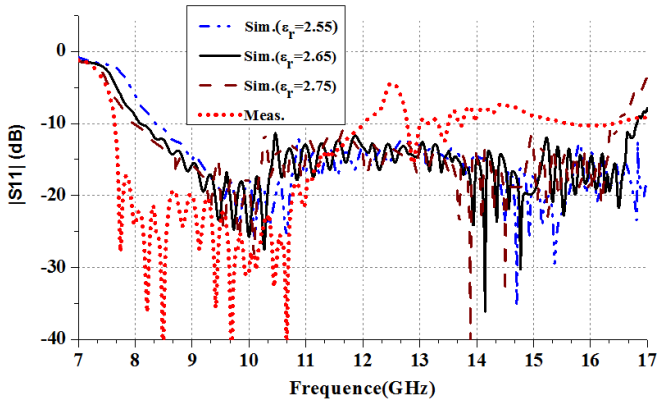

Fig. 12 Simulated reflection coefficient versus frequency with different ε_r.

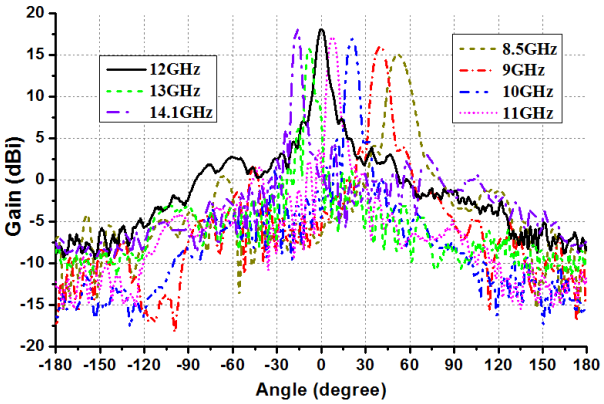

Fig.13 Measured gain patterns of beam steering.

Fig. 13 plots the measured beam steering patterns depending on different frequencies. The measured scanning angles is from -16.8° to 52.2° with the frequency decreasing from 14.1 GHz to 8.5 GHz. The measured and simulated scanning angle and the gain versus the frequency are illustrated in Fig. 14. The trends of the measured scanning angle agree well with that of the simulated one. The measured gain decreases from 0.4 dBi to 1.68 dBi between 8.5 and 14.1 GHz except for 2.96 dBi at 13 GHz. The decrease of the measured gain mainly comes from measurement error and the deterioration of the impedance match.

The measured characteristics of the SIW-CTS based FSA are summarized in TABLE II. At the broadside of 0°, the gain is 18.1 dBi, the sidelobe level is -11.4 dB, and the 3dB beam width

is 6.5°. The front-to-back ratios are higher than about 32 dB within the steering range. With the frequency decreasing, the 3dB beam width increase from 5.3° to 12.9° and the gain decreases from 18.1 dBi to 15.1 dBi.

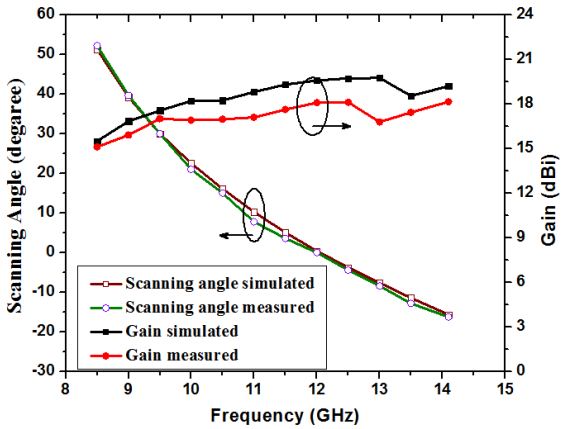

Fig. 14 Measured and the simulated scanning angle with the frequency.

TABLE II
MEASURED CHARACTERISTICS OF 16-ELEMENT SIW-CTS ARRAY

Frequency (GHz)	Scanning Angle(°)	Gain (dBi)	1st side lobe (dB)	F/B (dB)	3 dB BW(°)
8.5	52.2	15.1	-11.7	32.1	12.9
9	39.6	15.9	-11.5	34.8	10.0
9.5	30.8	17.0	-13.1	33.1	8.6
10	23.3	17.0	-12.4	51.3	7.6
10.5	14.8	17.0	-11.7	34.6	6.7
11	7.2	17.1	-13.7	44.3	6.4
11.5	3.6	17.6	-11.0	40.0	6.1
12	0	18.1	-11.4	31.7	6.5
13	-8.4	15.8	-12.5	35.0	5.6
14.1	-16.8	18.1	-8.9	32.8	5.3

TABLE III
PERFORMANCE COMPARISON OF FLAT FSAS

Ref.	Freq. range (GHz)	Scanning Angle range(°)	Peak Gain (dBi)	Sizes (λ_0) (L×W×H)
[4]	9.6-10.2	-25~25	8.1	1*19 array
[5]	8.75-12.25	-10~10	16-20.6	4.29×4.29×0.18
[6]	8.9- 10.6	-27.5~+46	13-15.5	8.7×1.5×0.04
[7]	8-13	-72~+75	9.6-12.6	6.0×0.7×0.032
[8]	0.93-3.65	-30~15	6.0-8.0	0.059×0.047×0.004
[16]	27-36	-43~3	11.6-17.8	13.5×2.1×0.22
This work	8.5-14.1	-16.8~52.2	15.1-18.1	11.7×1.28×0.24

λ_0 is the wavelength at the center frequency.

The most virtue of the FSA array is that the beam scanning is achieved by frequency varying within the operation band, and no phase shifter and mechanical adjusting are required. TABLE III summaries the performance comparison of the published flat FSA arrays. The FSA array in [5] has a little high gain but the scanning angle range is only 20°. The array in [7] has the most scanning range of 147° and a relative small size but the gain is very low. The antenna array size in [8] is very small while the maximum gain of 6-element array is only 8.0 dBi. The proposed SIW-CTS base FSA has a higher gain and a broad scanning range considering the array apertures.

V. CONCLUSION

A FSA based on SIW-CTS covering X/Ku band is presented. One parabolic reflector realized by SIW is designed and employed as the broadband linear source. The beam steers from 52.2° to -16.8° with the frequency increasing from 8.5 to 14.1 GHz, which is the 3-dB gain bandwidth. This FSA has high frond-to-back ratio over 32 dB and low first sidelobe of about -11 dB. The gain could be improved by increasing the length of the CTS stubs and the element number. This SIW-based FSA could also be realized by metal processing so it is suitable for the millimeter-wave applications. The FSA has a compact size, light weight, a simple structure and low cost, thus it could be potentially useful for both civilian and military applications (e.g. Satcom on the move system).

REFERENCES

[1] Y. Rahmat-Samii and A. C. Densmore, "Technology trends and challenges of antennas for satellite communication systems,"IEEE Trans. Antennas Propag., vol. 63, no. 4, pp.1191-1204, 2015.

[2] W. Imbraile, S. Gao and L. Boccia (eds), Space Antenna Handbook, John Wiley & Sons, 2012.

[3] F. S. Johansson, L. G. Josefsson, and T. C. Lorentzon, "A novel frequency-scanned reflector antenna,"IEEE Trans. Antennas Propag., vol. 37, no. 8, pp.984-989, 1989.

[4] M. Danielsen and R. Jorgensen, "Frequency scanning microstrip antennas," IEEE Trans. Antennas Propag., vol. AP-27, no. 2, pp.146-150, Mar. 1979.

[5] M. M. Bilgic and K. Yegin, "Wideband offset slot-coupled patch antenna array for X/Ku-band multimode radars," IEEE Antennas Wireless Prop. Lett., vol. 13, pp. 157-160, 2014.

[6] L. Cui, W. Wu, and D.-G. Fang, "Printed frequency beam-scanning antenna with flat gain and low sidelobe levels,"IEEE Antennas Wireless Prop. Lett., vol. 12, pp. 292-295, 2013.

[7] Nasimuddin, Z. N. Chen, and X. Qing,"Tapered composite right/left handed leaky-wave antenna for wideband broadside radiation,"Microw. Opt. Technol. Lett., vol. 57, no. 3, pp. 624-629, 2015.

[8] M. Alibakhshi-Kenari, A. Andujar, andJ. Anguera,"New compact printed leaky-wave antenna with beam steering,"Microw. Opt. Technol. Lett.,vol. 58, no. 1, pp.215-217, 2016.

[9] W. W. Milroy, "Continuous transverse stub (CTS) element devices andmethods of making same," U.S. Patent5266961, 1991.

[10] W. Kim and M. F. Iskander, "A new coplanar waveguide continuoustransverse stub (CPW-CTS) antenna for wireless communications,"IEEE Antennas Wireless Prop. Lett., vol. 4, pp. 172-174, 2005.

[11] R. Isom, M. F. Iskander, Z. Yun, and Z. Zhang, "Design and developmentof multiband coaxial Continuous Transverse Stub (CTS) antennaarrays," IEEE Trans. Antennas Propag., vol. 52, no. 8, pp. 2180-2184, 2004.

[12] P. J. V. Prakash and R. Srinivasan, Miniaturised multiband two-element coaxial continuous transverse stub antenna for satellite C-band applications, IET Microw. Antennas Propag., vol. 8, no. 7, pp. 474-481, 2014.

[13] Y. Li, M. F. Iskander, Z. Zhang, and Z. Feng, “A new low cost leakywave coplanar waveguide continuous transverse stub antenna array using metamaterial-based phase shifters for beam steering, IEEE Trans. Antennas Propag., vol. 61, no. 7, pp. 3511-3518, 2013.

[14] M. Ettorre, F. F. Manzillo, M. Casaletti, R. Sauleau, L. Le Coq, and N. Capet,“Continuous transverse stub array for Ka-band applications,”IEEE Trans. Antennas Propag., vol. 63, no. 11, pp.4792-4800, 2015.

[15] X.-X. Yang, L. Di, Y. Shen and J. Huang, “A Compact beam steering planar array with broadband and high gain,” Int. Symp. Antennas Propag. (ISAP), IEEE, November, 2015. PP.1-3.

[16] Hyeonhyeong Choe and Sungjoon Lim, “Millimeter-Wave Continuous Transverse Stub (CTS) Antenna Array Using Substrate Integrated Waveguide (SIW) Technology”, IEEE Trans. Antennas Propag., vol. 62, no. 11, pp. 5497-5503, 2014.

[17] Zhenxin Hu and Zhongxiang Shen, “Wideband flush-mountedsurface wave antenna” IEEE Trans. Antennas Propag., vol. 63, no. 6, pp.2430-2438, 2015.

[18] Y. Cassivi and K. Wu, “Dispersion characteristics of substrate integrated rectangular waveguide,” IEEE Microw. Wireless Compon. Lett., vol. 12, no. 9, pp. 333-335, Sep. 2002.

[19] Ansoft High Frequency Structure Simulator (HFSS) ver. 12, AnsoftCorp., 2011.

[20] D. Pozar, Microwave Engineering, John Wiley & Sons , Inc, pp. 112-120, 1998.